Marine Environmental Research 218 (2026) 107987

Contents lists available at ScienceDirect

Marine Environmental Research

journal homepage: www.elsevier.com/locate/marenvrev

Seasonal characterisation of iron-binding ligands in the South Atlantic sector of the Southern Ocean (Scale cruises, 2019)

V. Coussy [a], J.M. Santana-Casiano [a], M. González-Dávila [a], D. González-Santana [a], T.N. Mtshali [b], T.J. Ryan-Keogh [c], S. Samanta [d,1], A.N. Roychoudhury [d], A.G. González [a,*]

[a] Instituto de Oceanografía y Cambio Global, IOCAG, Universidad de Las Palmas de Gran Canaria, ULPGC, Las Palmas de Gran Canaria, Spain
[b] Department of Forestry Fisheries and Environment, Oceans and Coast, Cape Town, South Africa
[c] Southern Ocean Carbon-Climate Observatory, CSIR, Cape Town, South Africa
[d] Center for Trace Metal and Experimental Biogeochemistry (TracEx), Stellenbosch University, Stellenbosch, South Africa

ARTICLE INFO

Keywords:
Iron-binding ligands
Trace metals
Southern ocean
Island mass effect
GEOTRACES

ABSTRACT

The Southern Ocean (SO) is an essential oceanographic region to fully understand the iron (Fe) biogeochemical cycle. This work presents the first study of the Fe-binding ligands (L_{Fe}) concentrations and their conditional stability constant ($K^{cond}_{Fe'L}$) in the South Atlantic sector of the SO in winter and spring of the same year, determining the importance of L_{Fe} sources and sinks in the region. Along the transect, the L_{Fe} concentrations ranged from 0.74 to 2.42 nmol L^{-1} (mean = 1.29 nmol L^{-1}, n = 99) in winter and 0.57-2.03 nmol L^{-1} (mean = 1.18 nmol L^{-1}, n = 113) in spring. The log $K^{cond}_{Fe'L}$ ranged from 9.71 to 11.38 in winter and 9.75-11.21 in spring. Low L_{Fe} concentrations (winter: 0.89; spring: 0.93) and log $K^{cond}_{Fe'L}$ (winter: 10.06 nmol L^{-1}; spring: 9.99 nmol L^{-1}) were measured in the marginal ice zone (MIZ), where seasonal sea-ice cover limits ligand production by reducing biological and atmospheric inputs and trapping ligands during ice formation. In contrast, the highest L_{Fe} concentrations occurred in deep waters near Bouvet Island were shallower in winter (1000-1500 m; 2.42 nmol L^{-1}) compared to spring (1500-2000 m; 2.03 nmol L^{-1}) and associated with higher log $K^{cond}_{Fe'L}$ (winter: 11.24; spring: 10.83). These maxima reflect enhanced remineralisation, sediment resuspension, and the island mass effect on the Fe-binding ligands dynamics in the Southern Ocean. A significant positive correlation between L_{Fe} and apparent oxygen utilisation ($\rho = 0.517$, $p < 0.001$) confirms the key role of microbial remineralisation in ligand production in deep waters. Overall, seasonal differences in Fe-organic speciation were driven mainly by variations in ligand abundance rather than binding strength, shaped by the interplay of physical circulation, biological activity, and remineralisation.

1. Introduction

The Southern Ocean (SO) is a key oceanographic region due to its influence on global circulation and climate (Rintoul et al., 2001). However, the SO has not been studied during different seasons because of its geographic isolation, especially in winter due to the sea ice extension. It is known for its strong currents, such as the Antarctic Circumpolar Current (ACC), and significant fronts that have impacts on the iron (Fe) biogeochemical cycle, as well as on the biological activity (Klunder et al., 2011). Fe is essential for phytoplankton growth and shapes the composition of the plankton community due to its role in enzymatic reactions (Moore et al., 2001). The SO is recognised as one of the most important High Nutrient Low Chlorophyll (HNLC) areas, due to Fe limitation of phytoplankton growth (Boyd et al., 1979). As a result, the Fe biogeochemical cycle in the SO is essential and has a global impact (Sarmiento et al., 2004). Variation in Fe availability can stimulate phytoplankton growth and net primary production, potentially influencing carbon export through the biological carbon pump; however, it is not always translated into efficient transfer of carbon to the deep ocean (Tagliabue et al., 2014). While it is well-established that the spatial patterns of blooms in the SO are influenced by the Fe bioavailability (Pollard et al., 2009), the seasonal variations and characteristics

This article is part of a special issue entitled: Marine Processes and Humans MERE published in Marine Environmental Research.

* Corresponding author.
E-mail address: aridane.gonzalez@ulpgc.es (A.G. González).
[1] Present address: School of Geosciences, University of Witwatersrand, Johannesburg, South Africa.

https://doi.org/10.1016/j.marenvres.2026.107987
Received 12 June 2025; Received in revised form 9 March 2026; Accepted 12 March 2026
Available online 17 March 2026

of these blooms, including both consistent and inconsistent seasonal cycles, indicate the presence of distinct processes governing their supply (Thomalla et al., 2023).

The Fe biogeochemical cycle in the SO is constrained by its sources and sinks, which are heavily influenced by the existing water masses and hydrographic conditions (Thuróczy et al., 2011). In surface waters of this region, aerosol deposition (Klunder et al., 2011), upwelling (Klunder et al., 2011), ice melting (Croot et al., 2004; Smith et al., 2022), and shelf inputs (Marsay et al., 2014) are the major external sources of Fe. While water mixing, sediment leaching, and hydrothermal events are the major internal Fe sources in deep waters (Klunder et al., 2011). Furthermore, winter entrainment due to convective mixing plays a key role in replenishing the subsurface Fe reservoir, which potentially supports the initiation of the spring phytoplankton bloom when the mixed layer shoals (Tagliabue et al., 2014). Additionally, storm-driven entrainment events can episodically deepen the mixed layer, supplying pulses of Fe to surface waters and influencing bloom development (Nicholson et al., 2019). As a result, Fe concentrations in the Atlantic sector of the SO range between 0.1 and 0.7 nmol L^{-1} in surface waters, and around 0.5 nmol L^{-1} in deep waters (Thuróczy et al., 2011; Croot et al., 2004; Klunder et al., 2014) and reach up to 0.8 nmol L^{-1} close to the sediment bed (Klunder et al., 2011, 2014).

In the ocean, up to 99% of the dissolved Fe (dFe) is strongly complexed with organic compounds (known as iron-binding ligands (L_{Fe})) (Arnone et al., 2022; Boye et al., 2001; Gledhill and Buck, 2012; Rue and Bruland, 1995). This enhances the Fe solubility, preventing it from forming Fe-hydroxides and precipitating (Rue and Bruland, 1995). This also increases the residence time of Fe in surface water (Tagliabue et al., 2019), reduces Fe^{3+} to Fe^{2+} (Santana-Casiano et al., 2014), and increase its bioavailability to phytoplankton and bacteria in a limiting environment (Hassler et al., 2011). L_{Fe} can be classified according to the log $K^{cond}_{Fe'L}$ and are generally divided into two categories based on their strength: strong ligands (L_1), with log $K^{cond}_{Fe'L} > 12$, and weak ligands (L_2), with log $K^{cond}_{Fe'L} < 12$ (Gledhill and Buck, 2012; Rue and Bruland, 1995). These ligands are tentatively linked to functional groups or organic molecules. For example, siderophores are classified as L_1-type ligands (Rue and Bruland, 1995; Witter et al., 2000), humic substances and polyphenols are L_2-type ligands (Hassler et al., 2011, 2025; Rico et al., 2013).

The Antarctic shelf can impact the L_{Fe} cycle by providing a substantial number of organic compounds and humic substances through soil leaching or the sea ice melting (Gledhill and Buck, 2012; Genovese et al., 2022). In the open ocean, one of the main sources of L_{Fe} in the surface water is atmospheric dust deposition (Gledhill and Buck, 2012). Other sources include cell rupture following grazing (Sato et al., 2007), viral lysis (Poorvin et al., 2011), organic matter transformation (Gerringa et al., 2006), and phytoplankton exudates (Santana-Casiano et al., 2014; Rico et al., 2013). In response to Fe stress, prokaryotes can also produce specific ligands such as siderophores (Geider, 1999) or polyphenols (Rico et al., 2013). In addition, abiotic and biological processes can be sources of dissolved ligands in the form of amorphous inorganic phases or as strong organic chelators (Santana-Casiano et al., 2014; Boye et al., 2005). Hydrothermal vents and the sediments are also sources of L_{Fe} in deep waters (Gerringa et al., 2008). In the photic layer, photoreduction (Duan et al., 2017) and phytoplankton uptake (Croot et al., 2004; Boye et al., 2001) can both act as sinks for L_{Fe}. Finally, bacterial activity can also modulate L_{Fe} throughout the water column via remineralisation processes, acting either as a sink (through the degradation of organic ligands) or as a source of new binding sites via microbial processing of Dissolved Organic Matter (DOM) (Boye et al., 2001; Lacan et al., 2008).

Despite the importance of the Fe biogeochemical cycle in the SO, there is a lack of information about L_{Fe} and log $K^{cond}_{Fe'L}$ distribution in the region, especially in winter and spring. To close this gap, the objectives of this study are to characterise the seasonal and vertical distributions of L_{Fe} and log $K^{cond}_{Fe'L}$, and assess their variability across water masses, geographic zones, and stations during winter and spring in the Atlantic Sector of the Southern Ocean. This information is crucial for understanding the dynamics of the Fe biogeochemical cycle in the SO.

2. Materials and methods

2.1. Sampling strategy and study area

The seawater samples were collected during the SCALE 2019 cruises in early winter (18th July to August 12, 2019) and spring (12th October to November 20, 2019) on-board RV SA Agulhas II along the Good Hope transect (GEOTRACES - GIPY05) extending from Cape Town to the sea-ice edge reaching GT1 (55.98°S, 0°E) in winter and MIZ1 (57.57°S, 0°E) in spring (Fig. 1). During winter cruise, samples were collected throughout the water column from surface (25 m) down to 4500 m, whereas in spring, the sampling strategy focused on the upper 2000 m to obtain a higher vertical resolution in the surface and mesopelagic layers where most biogeochemical processes are concentrated. Additionally, not all stations could be sampled in winter due to adverse weather conditions. Stations from GT1 to GT7 were sampled during both winter and spring legs. In spring, five additional stations GT4, GT8, GT9, GT10, and MIZ1, were sampled. The crossover stations (GT1, GT2, GT3, GT5, GT6 and GT7) were located at the same latitudes and longitudes in both seasons. However, the sampling depths were not identical, as they were determined from in situ hydrographic and biogeochemical profiles (e.g., temperature, salinity, dissolved oxygen, and chlorophyll-*a* fluorescence) to target characteristic water masses and biogeochemical features (e.g., oxygen minimum, chlorophyll-*a* maximum).

Sample collection and processing was conducted following GEOTRACES protocols (Cutter et al., 2017; Cutter and Bruland, 2012). Seawater samples for L_{Fe} were collected from the trace metal clean 24 x 12 L GoFlo bottles mounted on an epoxy coated aluminium frame trace metal clean rosette equipped with Seabird CTD unit (SeaBird 911plus) attached to a conducting Kevlar cable. Once recovered, GoFlo bottles were quickly transported into a trace clean containerised laboratory equipped with HEPA filtered air circulation system for subsampling and processing. The L_{Fe} samples were collected by filtering seawater through 0.2 µm pore size capsule filters (Acropack, Separations) into 250 mL acid cleaned Low Density Polyethylene (LDPE) bottles, after rinsing the bottles 3 times with seawater sample before being filled. The samples were then double bagged and preserved frozen at −20 °C until analysis in a shore-based laboratory.

2.2. Instruments and reagents

The voltammetric equipment included a Potentiostat/galvanostat (Metrohm) paired with an IME 663 interface and a 663 VA Stand Metrohm Autolab, equipped with a hanging mercury drop electrode (Metrohm) having a drop surface area of approximately 0.25 mm^2. The reference electrode was double-junction, Ag/AgCl, 3 mol L^{-1} KCl, with a salt bridge also containing 3 mol L^{-1} KCl and a glassy carbon electrode served as a counter. Samples were stirred using a PTFE Teflon stirrer (3000 rpm). In order to minimise the electrical noise, a current filter (Fortress 750, Best Power) was connected to the equipment.

The buffer stock solution consisted of 1.0 mol L^{-1} boric acid (Suprapur, Merck) in 0.35 mol L^{-1} ammonia (Suprapur, Merck), which was cleaned overnight, stirring in the presence of 100 µmol L^{-1} of MnO_2 and subsequently filtered through a 0.2 µm filter (Millipore, GSWP, 25 mm) (Lucia et al., 1994). Several tests were performed to verify that the buffer was not contaminated. A 0.01 mol L^{-1} stock solution of TAC (2-(2-thiazolylazo)-p-cresol; Sigma-Aldrich) was freshly prepared each week in Methanol >99.9% (Honeywell), following the method of Croot and Johansson (2000). Fe stock solutions were monthly prepared from atomic absorption spectrometry standard solutions (Fluka, 1001 mg L^{-1}), diluted with wMQ-water, and acidified with 100 µL of ultrapure 12.8 mol L^{-1} HCl. The final concentrations in the stock solutions were as

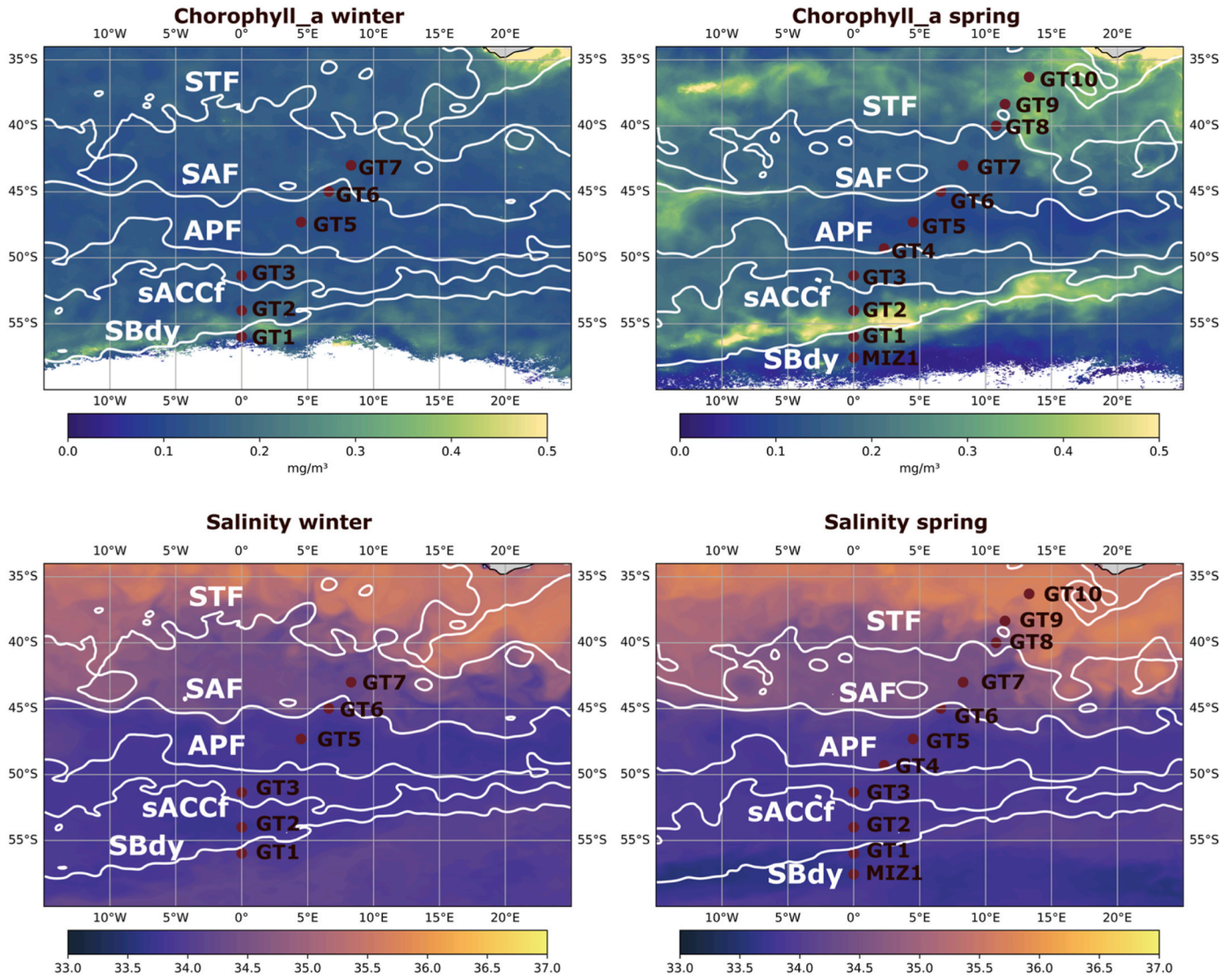

Fig. 1. Ocean colour chlorophyll-*a* concentration (mg m^{-3}, top panels) and sea surface salinity (bottom panels) averaged for winter (left, 18 July-12 August 2019) and spring (right, 12 October-20 November 2019). Sampled stations are shown as red dots (GT and Marginal ice zone (MIZ)) where L_{Fe} samples were collected. Fronts are indicated: STF = Subtropical Front; SAF = Subantarctic Front; PF = Polar Front; sACCf = Southern ACC Front; SBdy = Southern Boundary of the ACC. (For interpretation of the references to colour in this figure legend, the reader is referred to the Web version of this article.)

follows: Fe_1 = 180000 nmol L^{-1}; Fe_2 = 1800 nmol L^{-1}; Fe_3 = 900 nmol L^{-1}; Fe_4 = 90 nmol L^{-1}. All stock solutions were stored in the dark at 4 °C when not in use.

2.3. Theory

In a natural seawater sample, dFe was defined as the sum of organic species (FeL) and inorganic species, hereafter referred to as labile dFe (Fe').

$$[dFe] = [Fe'] + [FeL] \quad (1)$$

The labile iron concentration, denoted as [Fe'], refers to the total of all inorganic species, including Fe^{3+}. Iron bound to the binding sites of organic ligands (L) is represented as [FeL]. The reaction between Fe' and the labile organic binding site of natural binding ligands (L') can be described by the following reaction:

$$Fe' + L' \rightleftharpoons Fe'L \quad (2)$$

The affinity (strength) of a binding ligand is characterised by the conditional stability constant of this complex ($K^{cond}_{Fe'L}$), which can be determined using the following equation:

$$K^{cond}_{Fe'L} = \frac{[FeL]}{[Fe'][L']} \quad (3)$$

Where [L'] corresponds to the concentration of organic binding sites available to bind Fe, expressed as nmol eq Fe L^{-1}, rather than the absolute concentration of ligand molecules.

The concentration of free Fe^{3+} can be calculated from [Fe'] using the inorganic side reaction coefficient ($\alpha_{Fe'}$):

$$[Fe'] = \alpha_{Fe'} \cdot [Fe^{3+}] \quad (4)$$

The conditional stability constant can be determined with the ionic metal (Fe^{3+}) as shown below:

$$K^{cond}_{Fe^{3+}L} = \alpha_{Fe'} \cdot K^{cond}_{Fe'L} \quad (5)$$

The complexation capacity of dissolved ligands to bind with Fe is represented by the reactivity of the iron with natural binding ligands, denoted as f to avoid confusion with the side reaction α (Arnone et al., 2022; Gledhill and Gerringa, 2017). This coefficient can be estimated for

both Fe' and Fe^{3+} as demonstrated below:

$$f_{Fe'L} = K^{cond}_{Fe'L} \cdot [L'] \quad (6)$$

$$f^{3+}_{Fe}L = K^{cond}_{Fe^{3+}L} \cdot [L'] \quad (7)$$

The concentration of free Fe-binding sites is represented by the excess ligand (eL_{Fe}) (Arnone et al., 2023), which indicates the saturation state of ligands. Thus, eL_{Fe} is defined as follows:

$$[eL_{Fe}] = [L_{Fe}] - [Fe'L] \quad (8)$$

To determine the Fe speciation using CLE-ACSV, a well-characterised artificial ligand (TAC) must be introduced, which reacts with Fe and competes with FeL to form a complex (FeTAC). The FeTAC complex could adsorb at the mercury drop electrode and was electroactive, meaning that Fe could be reduced within the complex, generating a current proportional to the amount of Fe reduced. Additional details on Fe speciation analysis using TAC are provided in Croot and Johanson (Croot and Johansson, 2000).

The ligand concentration and the conditional stability constant, which can be estimated through titration, are determined by the "detection window", also called the analytical window. The centre of the detection window (DW) corresponds to the side reaction coefficient for the FeTAC complex (α_{FeTAC}), defined as the product of the TAC concentration and the conditional stability constant for the FeTAC complex. A higher α_{FeAL} value indicates a stronger ability to form complexes and compete with other ligands, enabling the detection of stronger complexes (with higher $K^{cond}_{Fe'L}$ or K^{cond}_{Fe} values) but leading to a lower concentration of ligands (Gledhill and Buck, 2012; Lucia et al., 1994). The DW for Fe is defined as follows:

$$\alpha_{Fe\ (TAC)2} = \beta^{cond}_{Fe(TAC)_2} \cdot [TAC]^2 = DW \quad (9)$$

For TAC concentrations of 5 and 10 μmol L^{-1}, $\beta^{cond}_{Fe\ (TAC)2}$ has a value of $10^{12.42\pm0.30}$ (Croot and Johansson, 2000).

The voltammetry method does not provide direct information about the nature of the detected compounds. However, it allows for comparison of the conditional constants obtained with those of compounds previously characterised through incubation experiments or other processes. The result is a highly heterogeneous and complex set of compounds that constitutes the ligand pool in seawater. When applying the CLE-ACSV method, several assumptions must be considered to obtain information about the bulk ligand concentration and constants (Gerringa et al., 2021). As a result, the term "conditional" is employed to describe the stability constants determined by voltammetry under the specified experimental conditions.

2.4. dFe determination

To determine dFe concentrations, samples were measured in the TracEx laboratory, University of Stellenbosch (South Africa), following the method described in the literature (Samanta et al., 2021). Samples were analysed in duplicate bottles using an online SC-4 DX seaFAST S3 (ESI seaFAST) preconcentration unit (X30) coupled with a quadrupole inductively coupled plasma mass spectrometer (ICP-MS; Agilent® 7900). Briefly, 3 mL of seawater was taken up the seaFAST unit, buffered with an ammonium acetate buffer to a pH of 6.0 ± 0.2, and loaded onto a high-affinity metal chelating resin column (Nobias EDTriaA). The metal ions, including Fe, were bound to the resin and separated from the seawater matrix elements (e.g., sodium, chloride), which passed through the column. The metal ions were subsequently eluted in 5% nitric acid (Ultrapur HNO_3; Merck) from the resin column in low volumes (100 μL), resulting in a preconcentration factor of 30. On the ICP-MS, samples were introduced using a low self-aspirating perfluoroalkoxy nebuliser (PFA-ST microflow) with a flow rate of 0.4 mL min^{-1}. The accuracy of the dFe analysis was quantified by comparing the analysed values of NASS-7 certified reference materials (measured = 5.98 ± 0.10 nmol kg^{-1}; certified = 6.16 ± 0.47 nmol kg^{-1}), GEOTRACES GSC 1-19 (measured = 1.63 ± 0.10 nmol kg^{-1}; consensus = 1.63 ± 0.10 nmol kg^{-1}) and GSP 62 (measured = 0.21 ± 0.03 nmol kg^{-1}, consensus = 0.16 ± 0.05 nmol kg^{-1}) community reference materials. The method blank was determined by analysing 2% HCl (Ultrapur; Merck). The limit of detection was calculated as three times the standard deviation of the pre-concentrated blank (0.01 nmol kg^{-1}). These data have been validated and accepted within the GEOTRACES IDP framework, confirming their conformity with international quality standards for trace metals.

2.5. Fe-binding ligands determination

The Fe-organic speciation analysis was conducted via Cathodic Stripping Voltammetry (CSV) using the 2-(2-Thiazolylazo)-p-cresol (TAC) as a competing ligand (Croot and Johansson, 2000), under a laminar flow hood inside a clean room. To determine the Fe-binding ligands, 10 mL samples were pipetted into 12 Teflon PFA vials (15 mL volume; Savillex), including two blanks (Gledhill and Buck, 2012). The seawater sample was buffered to pH 8.2 by adding into each vial, 100 μL of boric acid (final concentration 10^{-2} mol L^{-1}), and the Fe concentration varied (from +0 to +12 nmol L^{-1}). After a 1-h equilibration period between Fe and natural ligands, the desired TAC concentration was added and left to equilibrate overnight (Croot and Johansson, 2000). The following day, the titration series was measured using a deposition potential of 0.4 V and an equilibration time of 120 s. Voltammetric measurements were performed in differential pulse mode, with a start potential of −0.43 V and a stop potential of −0.65 V. The step potential was −0.00255 V with a modulation amplitude of −0.02 V, a modulation time of 0.04 s, and an interval time of 0.08 s. The data were analysed using the complete complexation fitting model of the ProMCC software (Omanović et al., 2015).

2.6. Statistical analysis

Statistical analyses were applied to determine whether there are significant differences in parameters associated with L_{Fe} and log $K^{cond}_{Fe'L}$ between seasons, water masses, and geographic zones. Normality of the data was assessed using the Shapiro-Wilk test. L_{Fe} concentrations did not follow a normal distribution in either season, while log $K^{cond}_{Fe'L}$ values were normally distributed. Seasonal differences were tested using Student's *t*-test (when variances were equal) or Mann-Whitney tests (when assumptions were not met). Differences among water masses and geographic zones were assessed using the non-parametric Kruskal-Wallis test, followed by Dunn's post hoc test with Bonferroni correction when significant ($p < 0.05$). All statistical analyses were carried out in Python (SciPy, scikit-posthocs, seaborn).

3. Results

3.1. Hydrographic characteristics

The cruise track crossed several major fronts of the Antarctic Circumpolar Current (ACC). These fronts were identified using maps of absolute dynamic topography (MADT) from the CLS-AVISO product (Rio et al., 2011), combined with regional boundary definitions (Swart et al., 2010) corresponding to the time when the cruise crossed each front and were well described in a previous study (Ramalepe et al., 2024). The study area was characterized by the presence of five fronts (Fig. 1), the subtropical front (STF) (winter: 40.64°S, 10.32°E; spring: 40.59°S, 10.35°E), the subantarctic front (SAF) (winter: 44.25°S, 7.34°E; spring: 44.69°S, 6.90°E), the polar front (PF) (winter: 49.45°S, 2.15°E; spring: 49.29°S, 2.40°E), the southern ACC front (sACCf) (winter: 51.82°S, 0.88°E; spring: 52.37°S, 0.00°E) and the southern boundary of the ACC (SBdy) (winter: 55.75°S, 0.85°E; spring: 56.21°S, 0.10°E). Based on these fronts, four zones can be identified moving southward: the subtropical zone (STZ) located north of the STF, the

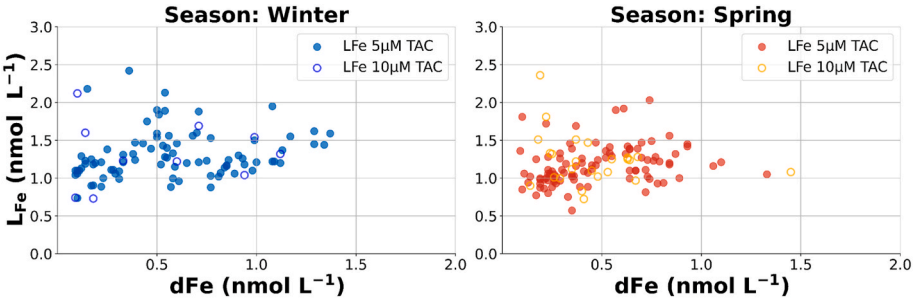

Fig. 2. Relationship between L_{Fe}, detected using 5 µmol L^{-1} of TAC (filled dots) and 10 µmol L^{-1} of TAC (empty dots), and dissolved iron (dFe) during winter (left, blue and purple) and spring (right, red and orange). Fe-ligand and dFe concentrations are expressed in nmol L^{-1}. (For interpretation of the references to colour in this figure legend, the reader is referred to the Web version of this article.)

subantarctic zone (SAZ) observed between STF and SAF, the polar frontal zone (PFZ) positioned between SAF and PF, and the Antarctic zone (AAZ) located south of the PF.

Observed water masses were characterised using potential temperature (θ), salinity (S), density (s_q) and Oxygen (Orsi et al., 1995) and were well described in the literature (Ringard et al., 2025). In the surface layer, Winter Waters (WW; $\theta < 0°$) and Antarctic Surface Waters (AASW; $S < 34.3$; $-1 < \theta < 0.5$ °C) dominated the southern stations, while the Sub-Antarctic Surface Waters (SASW; $33.8 < S < 34.3$, $5 < \theta < 12$ °C) was found between the SAF and PF north of the STF. Subtropical Surface Waters (STSW: $35.1 < S < 35.5$, $12 < \theta < 15.0$ °C) overlay thick layers of Sub-Antarctic Mode Waters (SAMW; $34.4 < S < 35.6$, $\theta < 10.5$ °C).

Intermediate waters were characterized by Antarctic Intermediate waters (AAIW; s_q 27.4 kg m^{-3}) with both Atlantic (A-AAIW; $34.25 < S < 34.3$) and Indian (I-AAIW; $34.3 < S < 34.6$) origin varieties, the latter reflecting the Agulhas leakage.

Deep waters include two types of cold and more saline North Atlantic Deep water (SE-NADW; $34.7 < S < 34.85$, $1.5 < \theta < 4$ °C and SW-NADW; Phosphate minimum) overlayed by Upper and Lower Circumpolar Deep Water (UCDW; $S < 34.6$; σ_θ isopycnal of 27.6 kg m^{-3}, O_2 min; LCDW; $S > 34.7$, σ_θ isopycnal of 27.8 kg m^{-3}). At the greatest depths, Antarctic Bottom Waters (AABW; $S > 34.75$; $\theta > -0.4$ °C) were observed.

This large-scale structure was consistent between winter and spring, with seasonal shoaling of Winter Waters and Antarctic Surface Waters in the south, and northward subduction of Sub-Antarctic Surface Waters and Sub-Antarctic Mode Waters into the subtropical zone.

3.2. *Detection window for L_{Fe}*

The first experimental series was focused on the selection of the DW to determine Fe-binding ligands and their conditional stability constant in winter and spring (Fig. 2). The titrations were carried out with 5 and 10 µmol L^{-1} of TAC, with the latter being used for open ocean samples (Thuróczy et al., 2011; Gerringa et al., 2008; Croot and Johansson, 2000). When 10 µmol L^{-1} of TAC was used, most winter samples tested (30 out of 43 analysed samples) and half of the spring samples were oversaturated. It is important to note that when the titration curve shows a linear slope (indicating oversaturation), it suggests that TAC has complexed all the added Fe, and/or the present ligands are out of the DW. The absence of contamination is corroborated by the dFe concentrations, measured by ICP-MS, consistently equal to or higher than those of Fe', determined by CLE-ACSV, as expected for uncontaminated samples. Moreover, the samples that were not oversaturated showed no significant different results between 5 and 10 µmol L^{-1} of TAC (paired *t*-test: $p = 0.643$; Fig. 2), demonstrating the first hypothesis. Accordingly, 5 µmol L^{-1} of TAC was found to be the most convenient concentration of TAC or DW to compare both seasons and the different seawater samples.

3.3. *General overview of the Fe-binding ligands and $K^{cond}_{Fe'L}$ distribution in the studied periods*

The L_{Fe} concentration in the whole region and both seasons ranged between 0.57 and 2.42 nmol L^{-1}, where higher values (winter: 2.42 nmol L^{-1}; spring: 2.03 nmol L^{-1}) were measured in deep waters (SW-NADW, UCDW and LCDW) (Figs. 3 and 4, and Table S1). The log $K^{cond}_{Fe'L}$ (Figs. 5 and 6, and Table S1) ranged between 9.71 and 11.38, with higher values observed between GT3 and GT5. In winter, L_{Fe} concentrations ranged between 0.74 and 2.42 nmol L^{-1}, and log $K^{cond}_{Fe'L}$ between 9.71 and 11.38. Whereas in spring, L_{Fe} concentrations ranged between 0.57 and 2.03 nmol L^{-1}, and log $K^{cond}_{Fe'L}$ between 9.75 and 11.21.

Along the transect, the L_{Fe} concentrations were significantly different between winter (0.74-2.18 nmol L^{-1}) and spring (0.57-1.81 nmol L^{-1}) (Mann-Whitney *U* test, $p = 0.041$; Figs. 1, 3 and 4, Fig. S2 and Table S1). In contrast, log $K^{cond}_{Fe'L}$ values showed no significant seasonal variation ($p = 0.394$). For both seasons, a minimum of L_{Fe} concentration was observed in surface waters (0-500 m), especially near the sea ice edge (GT1 winter: 0.89-1.10 nmol L^{-1}; GT1 spring: 1.04-1.33 nmol L^{-1}; MIZ1 spring: 0.93-0.94 nmol L^{-1}; Kruskal-Wallis, $p < 0.001$). Post-hoc Dunn tests confirmed that several pairwise contrasts were significant, particularly involving surface and intermediate water masses (AASW, SASW, WW) compared to deep and bottom waters (LCDW, UCDW, SW-NADW). In spring, lower L_{Fe} concentrations were also observed between GT4 and GT5 (0.75 nmol L^{-1}) and between GT8 and GT10 (0.57 nmol L^{-1}) (Mann-Whitney, $p = 0.001$; median 0.97 vs 1.18 nmol L^{-1}) compared to GT3 and GT6. For all stations and both seasons, log $K^{cond}_{Fe'L}$ (Figs. 5 and 6, and Table S1) values increased from the sea ice edge to the open ocean (Mann-Whitney *U* test, $p = 0.006$). The log $K^{cond}_{Fe'L}$ values varied significantly among zones (Kruskal-Wallis, $p = 0.001$), with the SAZ being significantly different from the AAZ and the SBdy. Lower log $K^{cond}_{Fe'L}$ values were observed for both seasons throughout the SBdy (GT1 winter: log $K^{cond}_{Fe'L}$ = 10.06-10.34; GT1 spring: log $K^{cond}_{Fe'L}$ = 9.99-10.13; MIZ1 spring: 10.38-10.55), while higher log $K^{cond}_{Fe'L}$ values were observed for both seasons between GT2 and GT6 (winter: log $K^{cond}_{Fe'L}$ = 11.38; spring: log $K^{cond}_{Fe'L}$ = 11.19). Additionally, in spring, weaker ligands were found across the GT9 (with log $K^{cond}_{Fe'L}$ = 9.86) and the GT7 (with log $K^{cond}_{Fe'L}$ = 9.79), and higher log $K^{cond}_{Fe'L}$ north of the GT10 (with log $K^{cond}_{Fe'L}$ = 11.21).

In the intermediate waters, the L_{Fe} concentrations were higher within AAIW and SAMW waters and reached maximum values in deep waters (UCDW, LCDW) between GT3 and GT5 (winter: 2.42 nmol L^{-1}; spring: 2.03 nmol L^{-1}). These observed concentrations are in association with a maximum of log $K^{cond}_{Fe'L}$ (winter: 11.38; spring: 11.21; Figs. 5 and 6). Another log $K^{cond}_{Fe'L}$ maximum was observed north of GT8 in spring (11.11), while lower log $K^{cond}_{Fe'L}$ (winter: 10.09; spring: 9.99) were observed between GT3 and GT1.

In the deep waters, the L_{Fe} concentration maximum were observed for both seasons near Bouvet island, located on the Southwest Indian Ridge (54.25°S, 3.22°E, next to GT2, winter: 2.42 nmol L^{-1}; spring: 2.03

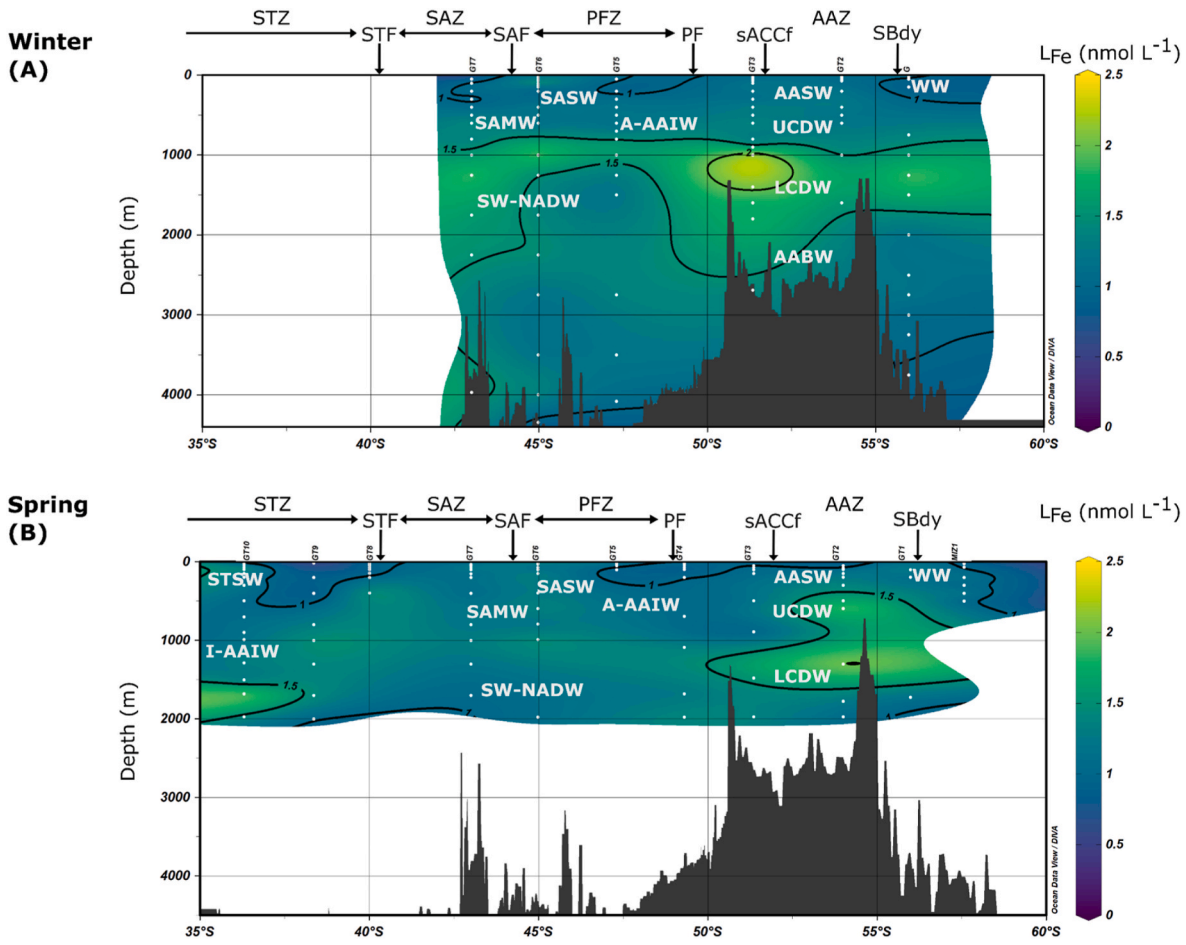

Fig. 3. Distribution of L_{Fe} (nmol L^{-1}) in winter (A) and spring (B) across the section.

nmol L^{-1}) within the SW-NADW and LCDW (Figs. 3 and 4, and Table S1) with statistical analysis confirming that concentrations in these water masses were significantly higher than those measured in other water masses along the transect (Mann-Whitney *U* test, Winter: $p = 0.0001$; Spring: $p = 0.042$). However, they were found at different depths, between 1000 and 1500 m in winter (>1.5 nmol L^{-1}; Fig. 3) and between 1500 and 2000 m in spring (>1.5 nmol L^{-1}; Fig. 3). Lower log $K^{cond}_{Fe'L}$ (Figs. 5 and 6, and Table S1) were observed during winter within the deep waters in GT1 (10.11-10.64) and next to GT2 (10.09). In spring, lower log $K^{cond}_{Fe'L}$ were also found near MIZ1 and GT1 (10.03-10.50) and in GT7 (9.75-10.63) throughout the SAMW and AAIW waters. These differences were statistically significant (Kruskal-Wallis $p < 0.001$ for both seasons), confirming that log $K^{cond}_{Fe'L}$ varied markedly between water masses. In contrast, higher log $K^{cond}_{Fe'L}$ values were consistently found between GT2 and GT5 (winter: 11.24; spring: 10.83), with post-hoc tests indicating significantly stronger ligand complexes in these central stations compared to GT1 and GT7 (Mann-Whitney, $p = 0.016$ in winter; $p = 0.006$ in spring).

Only winter stations were carried out deeper than 2000 m, where a second minimum of L_{Fe} concentration, ranging between 0.88 and 1.53 nmol L^{-1}, was observed specifically near GT1, GT5 and GT6 (0.96; 1.06; 0.88 nmol L^{-1}, respectively). Statistical analysis confirmed that these concentrations were significantly lower than those measured in other deep stations (Mann-Whitney *U* test, $p = 0.038$, median = 1.20 vs. 1.48 nmol L^{-1}), supporting the presence of a secondary L_{Fe} minimum at these depths. Low log $K^{cond}_{Fe'L}$ was equivalently found in GT1 (10.11), AABW (10.09), and in SW-NADW (9.71).

The L_{Fe} was compared against apparent oxygen utilisation (AOU) (Fig. 7), determined using the Gibbs Seawater package and calibrated CTD sensors from Ryan-Keogh (Ryan-Keogh, 2025a; Ryan-Keogh, 2025b) (CTD data from spring and winter, respectively), for both winter and spring samples to examine the potential relationship with the remineralisation processes in the region. Higher AOU and L_{Fe} were found in deep waters in both seasons (winter: 189.93 μmol kg^{-1}; spring: 185.88 μmol kg^{-1}) and particularly between GT3 and GT5 (winter: 154.81-182.54 μmol kg^{-1}; spring: 129.64-178.52 μmol kg^{-1}). Furthermore, high AOU values were observed for the waters deeper than 2000 m in winter (GT1-GT3: 174.17 μmol kg^{-1}; GT5-GT6: 163.46-166.87 μmol kg^{-1}; GT7: 159.66-166.87 μmol kg^{-1}). Statistical analyses revealed a significant overall correlation between L_{Fe} and AOU across the water column (Spearman $\rho = 0.517$, $p < 0.001$), with the relationship being strongest at intermediate depths (200-2000 m; $\rho = 0.36$-0.41, $p > 0.01$). In contrast, no significant relationship was observed in surface waters (0-200 m) or below 2000 m, where the limited number of data points precluded robust testing. Seasonal comparisons further showed no significant difference in L_{Fe} concentrations between winter and spring in the upper 200-1000 m, but a significant seasonal effect was detected at 1000-2000 m (*t*-test, $p = 0.004$), with higher L_{Fe} concentrations in spring. No significant seasonal difference was found at 0-200 m or in the deep waters below 2000 m.

4. Discussion

The L_{Fe} concentrations observed in the study ranged between 0.57 and 2.42 nmol L^{-1} (Figs. 3 and 4) and fall within the range of previously reported concentrations for the Southern Ocean. When comparing the mean value, they tend to be higher than those previously documented for the same water masses in different years, including different artificial

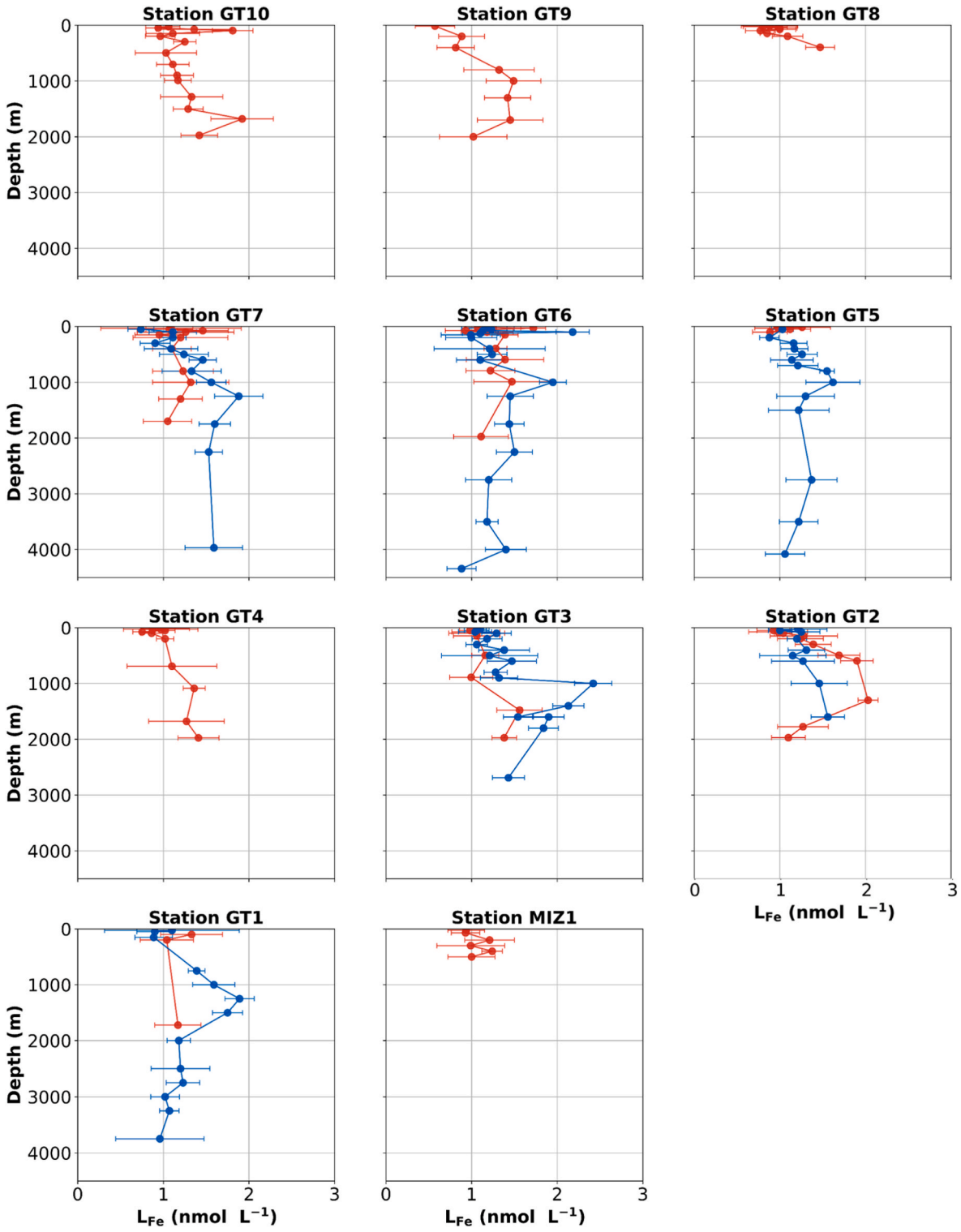

Fig. 4. Vertical profiles of L_{Fe} (nmol L^{-1}) in each station. Winter data are plotted as blue points, and spring data are presented in red points. (For interpretation of the references to colour in this figure legend, the reader is referred to the Web version of this article.)

ligands, and detection windows (Thuróczy et al., 2011; Croot et al., 2004; Boye et al., 2001, 2005) (Fig. 8). This contrast is particularly evident when comparing with earlier studies conducted along similar transects during summer (1999 and 2008; 0.37-3.00 nmol L^{-1}; DW NN 5 μmol L^{-1} (Croot et al., 2004; Boye et al., 2001); DW TAC 10 μmol L^{-1} (Thuróczy et al., 2011; Croot et al., 2004)) or spring (2000; 0.56-0.79 nmol L^{-1}; 10 μmol L^{-1} of TAC for DW (Boye et al., 2005) Table S2), which generally reported lower L_{Fe} concentration. In contrast, log $K'^{cond}_{Fe'L}$ (9.71-11.38) are consistently lower than literature values (summer: 11.0-13.0 (Croot et al., 2004; Boye et al., 2001); spring: 11.55-12.39 (Boye et al., 2005)), suggesting a predominance of weaker ligands (L_2-type) in our dataset. The log $K'^{cond}_{Fe'L}$ values observed in this study are consistent with the presence of humic-like substances, which are partly detected with TAC, and which are known to accumulate at depth as a result of microbial processing of organic matter during remineralisation processes. Other possible contributors include degradation products

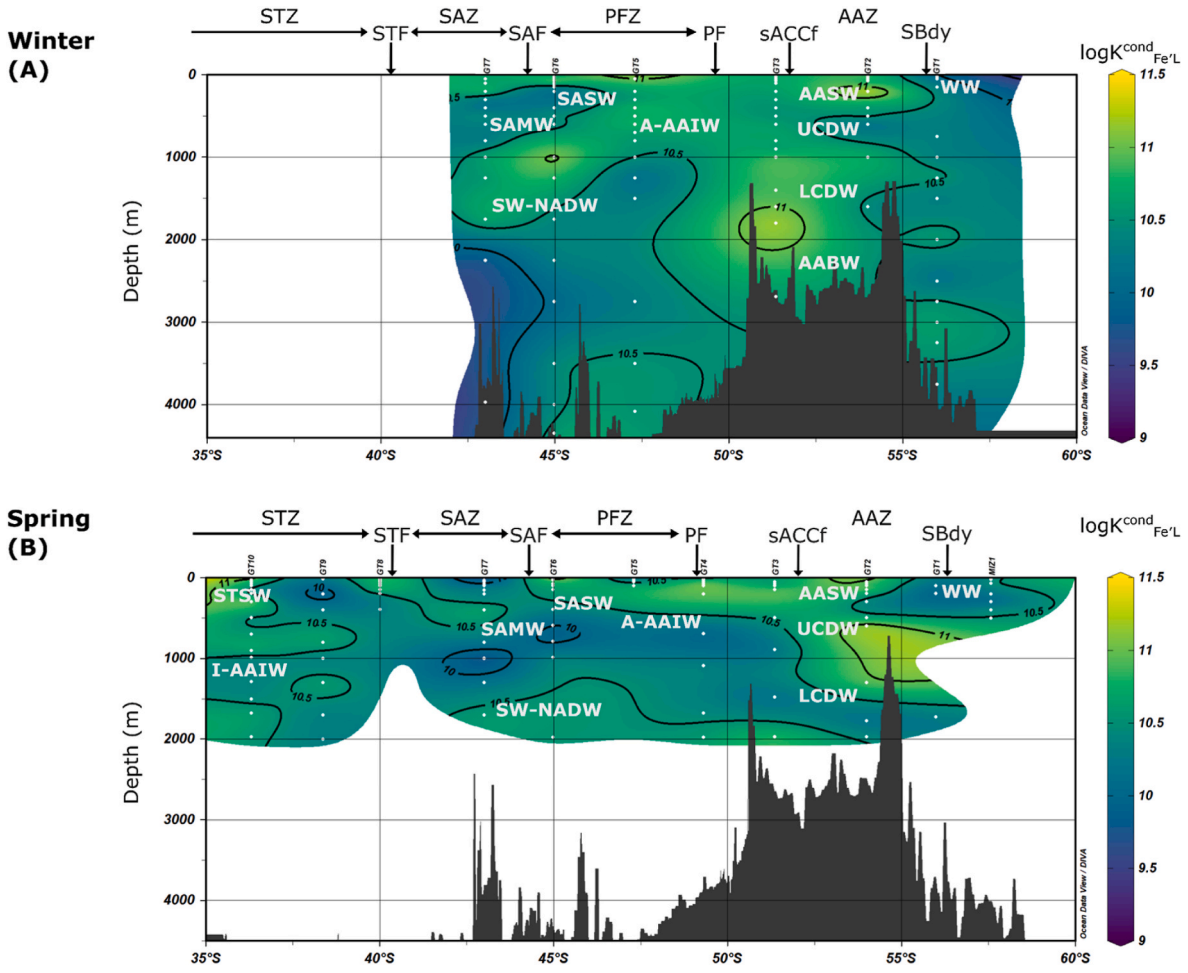

Fig. 5. Distribution of Log $K^{cond}_{Fe'L}$ in winter (A) and spring (B) across the section.

such as phaeophytin or polyphenols, which are derived from phytoplankton and are typically observed in surface and subsurface waters (Witter et al., 2000; Rico et al., 2013; Hassler et al., 2025). In contrast, the low log $K^{cond}_{Fe'L}$ values observed make it unlikely that siderophores such as enterobactin or alterobactin dominated the ligand pool.

This difference between the literature and our dataset in terms of L_{Fe} concentration and log $K^{cond}_{Fe'L}$ value can be attributed to different factors. First, the methodological differences, such as the choice of artificial ligands and detection windows, can influence ligand quantification and binding strength measurement. Second, our study uniquely includes winter data, a season characterised by reduced external inputs (e.g., atmospheric deposition, sea ice melt (Genovese et al., 2022; Demasy et al., 2024)) and biological activity highlighted by low and spatially homogeneous chlorophyll-*a* values during the winter season (Fig. 1). These conditions favour the accumulation of weaker, microbially derived or degradation-derived ligands (Croot et al., 2004; Rue and Bruland, 1995). To illustrate these trends, a water mass-based comparison (Fig. 8) reveals that the mean L_{Fe} and log $K^{cond}_{Fe'L}$ values vary significantly with season and depth, highlighting the combined influence of biogeochemical processes and oceanic circulation. These factors may also explain why many of our samples were oversaturated when we used the common DW (10 μM TAC), compared to what is generally reported in the literature. In addition, we should note that the samples have been collected in different sites, not the same stations.

4.1. Surface variability

In surface waters (0-500 m), L_{Fe} concentrations (0.57-2.18 nmol L^{-1}; Figs. 3 and 4) and their seasonal patterns reflect distinct source processes and transformation mechanisms. During winter, L_{Fe} concentrations (0.74-2.18 nmol L^{-1}) are coupled with low log $K^{cond}_{Fe'L}$ values (10.09-10.34; Figs. 5 and 6), indicating a predominance of weaker ligands. This pattern is consistent with reduced external inputs due to extensive sea ice cover, which limit atmospheric dust deposition and continental runoff, thereby minimising the supply of stronger ligands such as siderophores. Abiotic processes, including photoreduction of organic matter and sea ice formation, further promote the retention of weaker ligands, such as humic-like substances, in the dissolved phase (Croot et al., 2004; Rue and Bruland, 1995). For instance, at GT1 (55.98°S), L_{Fe} concentrations (0.89-1.10 nmol L^{-1}) and log $K^{cond}_{Fe'L}$ values (10.06-10.34) align with this trend, exhibiting low spatial variability due to wintertime homogenization of water masses (Genovese et al., 2022). This phenomenon is highlighted by low and spatially homogeneous chlorophyll-*a* concentrations (Fig. 1), consistent with reduced biological activity and the dominance of weaker ligands supplied by sea-ice processes.

In spring, L_{Fe} concentrations (0.57-1.81 nmol L^{-1}) remain within the same range as winter, but their spatial distribution and binding strengths display marked seasonal differences. Sea-ice melt releases both dissolved iron and fresh ligands, potentially including stronger siderophore-like compounds derived from under-ice microbial activity (Genovese et al., 2022). Concurrently, the resurgence of primary productivity in spring north of the SAF and in the MIZ, evidenced by satellite-derived chlorophyll-*a* data (Fig. 1), generates stronger ligands through phytoplankton exudates and cell lysis (Santana-Casiano et al., 2014; Rico et al., 2013; Poorvin et al., 2011). Atmospheric dust deposition, particularly from Patagonian sources, supplies iron alongside organic matter that can interact with the ambient ligand pool. While

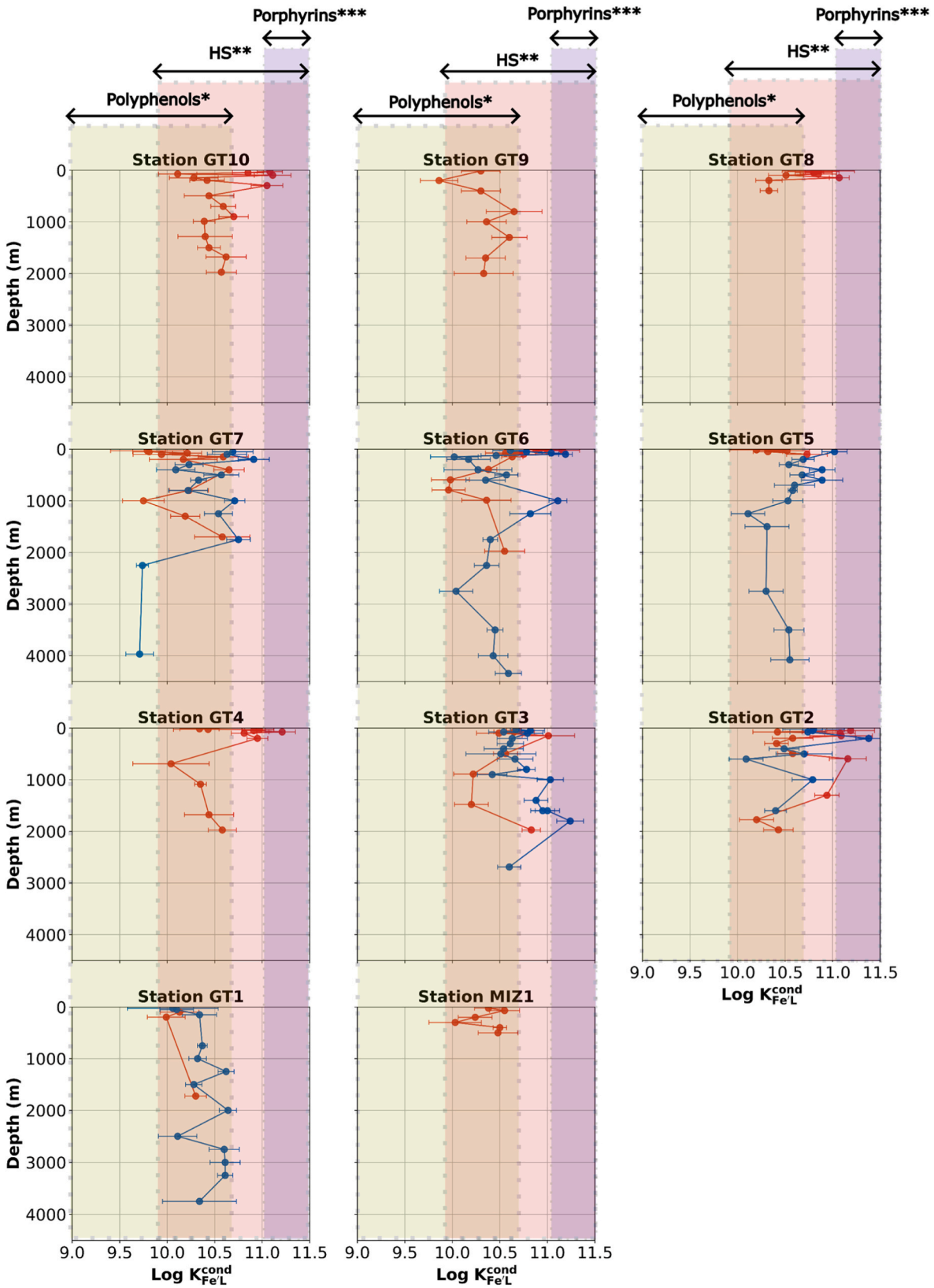

Fig. 6. Vertical profiles of log $K'^{cond}_{Fe'L}$ in each station. Winter data are plotted as blue points, and spring data are presented in red points. * (Hassler et al., 2011; Rico et al., 2013) ** (Hassler et al., 2025) *** (Witter et al., 2000). (For interpretation of the references to colour in this figure legend, the reader is referred to the Web version of this article.)

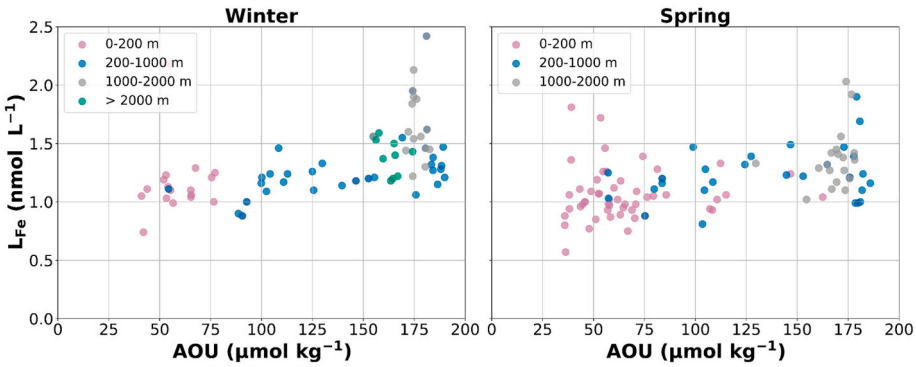

Fig. 7. L_{Fe} (nmol L^{-1}) against the AOU (µmol kg^{-1}) for winter (left) and spring (right). The green circles represent the samples from 0 to 200 m, the red circles from 200 to 1000 m, the blue circles from 1000 to 2000 m, and the black circles >2000 m. (For interpretation of the references to colour in this figure legend, the reader is referred to the Web version of this article.)

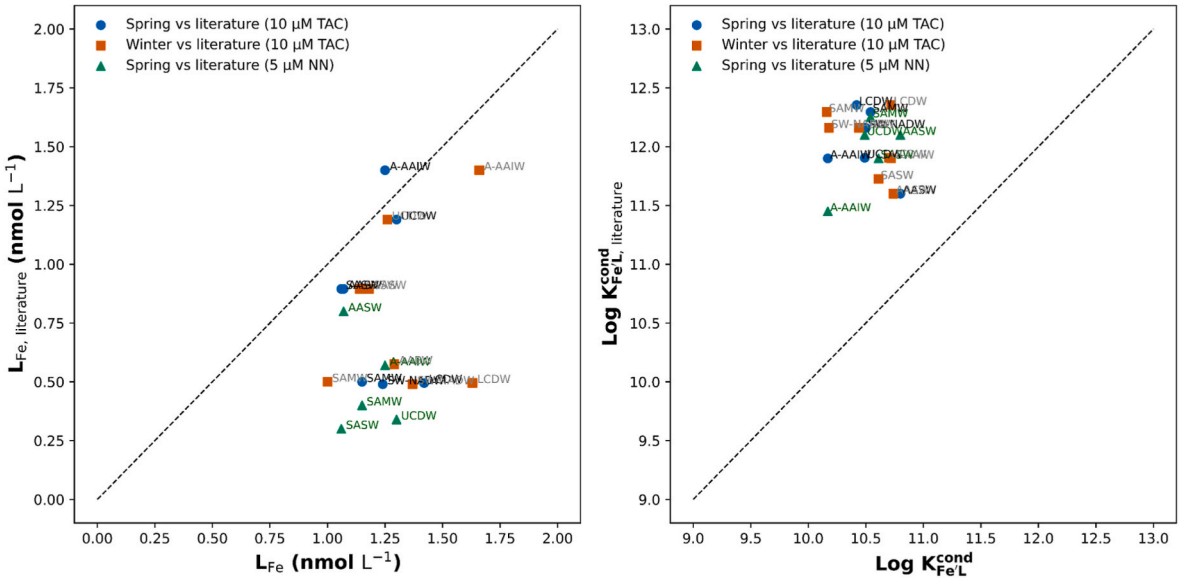

Fig. 8. Comparison of mean L_{Fe} (left) and log $K^{cond}_{Fe'L}$ (right) values from this study (winter and spring, x axes) with previously published data for similar water masses in the same region (y axes) (Thuróczy et al., 2011; Croot et al., 2004; Boye et al., 2001, 2005). Mean values from each dataset were averaged by water mass to facilitate comparison across studies. Symbols represent individual water masses; the dashed 1:1 line indicates perfect agreement between datasets.

dust itself is not a direct source of the ligands detected by CLE-ACSV, recent studies demonstrate that DOM enhances the dissolution and stabilisation of iron released from dust particles (Demasy et al., 2024). At GT1, sea ice melt leads to increased L_{Fe} concentrations (1.04-1.33 nmol L^{-1}) but decreased log $K^{cond}_{Fe'L}$ values (9.99-10.13), suggesting the release of weaker ligands during melt events. In contrast, the marginal ice zone (MIZ1, 57.57°S) exhibits lower L_{Fe} concentrations (0.93-0.94 nmol L^{-1}) but higher log $K^{cond}_{Fe'L}$ values (10.38-10.55), consistent with the presence of fresher, stronger ligands from melting sea ice (Genovese et al., 2022).

Spatial variability in ligand characteristics is particularly pronounced at oceanic fronts, where higher log $K^{cond}_{Fe'L}$ values (Figs. 5 and 6) were observed between the SBdy and the SAF (GT2-GT6) in both seasons (winter: 11.38; spring: 11.19) and north of the STF in spring (11.21 at GT10). These stronger ligands likely reflect enhanced biological activity and inputs from atmospheric dust deposition (Demasy et al., 2024), cell rupture following grazing (Sato et al., 2007), viral lysis (Poorvin et al., 2011), organic matter transformation (Gerringa et al., 2006), or phytoplankton exudates (Santana-Casiano et al., 2014; Rico et al., 2013). Conversely, in low-productivity zones such as the PFZ and STZ, L_{Fe} concentrations (Figs. 3 and 4) and log $K^{cond}_{Fe'L}$ values (Figs. 5 and 6) are minimal (L_{Fe} of 0.75 and 0.57 nmol L^{-1} respectively at GT4 and GT9; and log $K^{cond}_{Fe'L}$ of 9.79 and 9.86 respectively at GT7 and GT9), reflecting competition between ligand sources (e.g., dust deposition, biological exudates) and sinks (e.g., uptake, particulate scavenging).

Statistical analyses confirm that seasonal variability in L_{Fe} appear to be more strongly associated with changes in ligand pool size rather than binding strength, with significant differences between winter and spring. Seasonal differences were also evident in the SBdy where log $f_{Fe'L}$ minima occurred at GT1 and were lower in winter (1.05) than in spring (1.26), indicating a weaker ligand pool under reduced external inputs. In contrast, log $K^{cond}_{Fe'L}$ values remain stable across seasons, suggesting that shifts in iron speciation are more closely linked to ligand production and removal processes than to changes in ligand chemistry.

4.2. *Deep waters and remineralisation*

Between the surface minima and deep waters maxima, the intermediate waters appear to be a transition zone, characterised by increasing concentrations of L_{Fe}. The distribution of both L_{Fe} and log

$K^{cond}_{Fe'L}$ was strongly structured by water masses, underlining the importance of physical circulation and water mass history in shaping Fe speciation. Surface and intermediate waters showed the greatest contrasts relative to deep and bottom waters, consistent with their exposure to external Fe inputs, biological activity, and remineralisation. Finally, the two-way ANOVA confirmed that log $K^{cond}_{Fe'L}$ is structured primarily by water mass type, with a secondary contribution from seasonality. The significant interaction between season and water mass suggests that seasonal effects are not uniform across the water column but depend on the biogeochemical context of individual water masses. Together, these results emphasise that both vertical structure and seasonal dynamics need to be considered to understand Fe speciation in the Southern Ocean.

The highest L_{Fe} concentrations were found for both seasons in the deep waters (winter: 2.42 nmol L^{-1} at GT3; spring: 2.03 nmol L^{-1} at GT2), especially between the GT2 and GT4, and next to GT3 for winter (Figs. 3 and 4). Furthermore, the highest concentration of L_{Fe} was observed at different depths compared to previous studies. In this study, the maximum concentrations of L_{Fe} were found in winter around 1000-1500 m and in spring around 1500-2000 m, while in summer they were reported at 2000-2500 m (Thuróczy et al., 2011). This downward shift can be attributed to the seasonal changes in water mass circulation and mixing processes. The maxima L_{Fe} concentration (winter: 2.42 nmol L^{-1}; spring: 2.03 nmol L^{-1}; Figs. 3 and 4) consistently occurred within the SW-NADW and LCDW waters, where log $K^{cond}_{Fe'L}$ values were also elevated (winter: 11.24; spring: 10.83; Figs. 5 and 6), suggesting strong complexation capacity in these deep waters.

Enhanced remineralisation appears to be likely contributing to these maxima, as indicated by elevated AOU values (winter: 154.81-182.54 μmol kg^{-1}; spring: 129.64-178.52 μmol kg^{-1}) (Fig. 7), which denote active microbial oxidation of organic matter. This process releases ligands during the degradation of dissolved organic matter (DOM), thereby increasing L_{Fe} concentrations. In addition, the distribution of L_{Fe} can be influenced by physical mechanisms such as winter entrainment, diapycnal diffusion, vertical Ekman pumping, and lateral advection. These processes act to transport and mix water masses, which can redistribute dissolved ligands within and across density layers. For instance, winter entrainment and diapycnal diffusion enhance the vertical supply of ligands from deeper layers, whereas Ekman pumping and lateral advection contribute to their horizontal redistribution. Such mechanisms, well documented for other tracers in the Southern Ocean (e.g., for dissolved manganese (Ramalepe et al., 2024)), are therefore also likely to shape the observed vertical and lateral maxima of L_{Fe} in the SW-NADW and LCDW layers.

A complementary explanation for the elevated deep L_{Fe} near GT2-GT3 involves the island mass effect of Bouvet Island, well described in the literature as an important source of Fe to the surrounding waters (Gerringa et al., 2008). Local processes such as release of Fe from shelf, slope sediments transport, resuspension and lateral transport of particulate material, and enhanced remineralisation of island-derived organic matter (Boye et al., 2001; Lacan et al., 2008), likely contribute to elevated L_{Fe} concentrations observed near Bouvet Island. Although remineralisation represents a sink of organic matter, it simultaneously produces DOM that can be microbially processed, thereby increasing the abundance of iron-binding sites and thus contributing to higher L_{Fe} concentrations. This interpretation is consistent with our observations of a significant positive correlation between L_{Fe} and AOU across the water column (Spearman $\rho = 0.517$, $p < 0.001$), especially at intermediate depths (200-2000 m). In parallel, mixing processes, particularly in the ACC domain (Klunder et al., 2011), can redistribute these ligands laterally and vertically, contributing to their wider spread. Finally, the presence of suspended particulate matter (Tagliabue et al., 2019) may also enhance metal cycling through particle-ligand interactions, although its role in dissolved L_{Fe} variability remains secondary compared to remineralisation-driven DOM processing. These mechanisms collectively provide a plausible explanation for the elevated L_{Fe} concentrations observed near the island during our study.

In contrast to the high log $K^{cond}_{Fe'L}$ observed in the SW-NADW and LCDW, lower log $K^{cond}_{Fe'L}$ values were found at GT 1 (10.11-10.64) and GT2 (10.09) in winter, and at GT1, MIZ1 (10.03-10.50), and within the SAMW and AAIW at GT7 (9.75-10.63) in spring (Figs. 5 and 6). These values can be explained by the upwelling of deep waters near Antarctica and their advection northward, where most of the AASW subduct near the PF to form AAIW (Sarmiento et al., 2004). These low log $K^{cond}_{Fe'L}$ values can result from remineralisation process that increases the abundance of iron-binding sites through microbial alteration of DOM but can simultaneously reduce their overall binding strength (Boye et al., 2001; Lacan et al., 2008). This interpretation is supported by the significant positive correlation observed between L_{Fe} and AOU ($\rho = 0.517$, $p < 0.001$), particularly at intermediate depths, whereas no significant correlation was detected between log $K^{cond}_{Fe'L}$ and AOU. Such trends are consistent with microbial processing of DOM leading to the accumulation of ligands with phenolic and carboxylate functional groups, as reported in the DOM literature. In parallel, these waters are also characterised by a reduction in external sources, such as inputs from dust, sea ice, or lateral transport, which typically provide stronger ligands. The combination of enhanced remineralisation and limited external supply thus explains the observed increase in ligand abundance associated with lower conditional stability constants.

In winter, below 2000 m, the L_{Fe} concentrations were minimal at all stations (0.88-1.53 nmol L^{-1}) with the lowest values observed in the SBdy, PF and SAF (respectively 0.96, 1.06, and 0.88 nmol L^{-1}, Figs. 3 and 4; Mann-Whitney $p = 0.038$). Low log $K^{cond}_{Fe'L}$ was equally found in the SBdy (10.11), AABW (10.09), and in SW-NADW (9.71) (Figs. 5 and 6). These concentrations were found in older waters (AABW and SW-NADW), which have undergone a prolonged isolation from surface inputs, such as atmospheric deposits or biological activity, and extensive remineralisation, highlighted by high AOU values shown in Fig. 7 (AAZ: 174.17 μmol kg^{-1}; PFZ: 163.46-166.87 μmol kg^{-1}; SAZ: 159.66-166.87 μmol kg^{-1}) and lower log $K^{cond}_{Fe'L}$ (AAZ and SAZ: 10.09, Figs. 5 and 6). This reflects the persistence of weak, microbially altered ligands and the gradual loss of stronger complexes over time.

Finally, high L_{Fe} concentrations and log $K^{cond}_{Fe'L}$ were observed across the sACCf, likely reflecting sediment resuspension processes supplying dFe from bottom waters (Gerringa et al., 2008; Ardiningsih et al., 2021). Although these studies primarily focused on dFe, sediment resuspension and particle-associated processes may also contribute to the release of organic ligands or promote complexation in situ. Combined with the island mass effects, as previously discussed (Gerringa et al., 2008), these sediment-derived ligands could further enhance the supply of both Fe and organic matter from Bouvet Island, thereby supporting the elevated L_{Fe} levels observed at depth.

5. Conclusions

By combining high-resolution seasonal sampling and ligand speciation analysis, this study provides new insights into the processes controlling iron complexation in the Southern Ocean. This study presents the first comparison of Fe-binding ligand characteristics between winter and spring in the South Atlantic sector of the Southern Ocean. Distinct seasonal and vertical patterns were observed in both ligand concentrations (L_{Fe}: 0.57-2.42 nmol L^{-1}) and conditional stability constants (log $K^{cond}_{Fe'L}$: 9.71-11.38).

In surface waters (0-500 m), L_{Fe} and log $K^{cond}_{Fe'L}$ increased from the sea-ice edge toward the open ocean, consistent with the influence of seasonal sea-ice processes and biological production. During winter, weaker ligands are incorporated into sea ice, while spring melting and enhanced productivity release both stored and newly produced ligands,

expanding the ligand reservoir. Satellite chlorophyll-*a* patterns corroborate this seasonal shift, showing higher productivity and potential ligand release during spring.

In deep waters (>1000 m), L_{Fe} maxima were measured near Bouvet Island and within the SW-NADW and LCDW, where remineralisation and island mass effects sustain elevated ligand concentrations. The significant positive correlation between L_{Fe} and AOU ($\rho = 0.517$, $p < 0.001$) indicates that microbial processing of organic matter is a major source of ligands, while lower stability constants in aged waters (AABW, SW-NADW) reflect the accumulation of weaker, humic-like complexes.

Overall, this study shows that variations in dFe speciation appear to be more strongly associated with ligand abundance than with changes in binding strength, controlled by the interplay of physical circulation, biological activity, and remineralisation. These findings advance our understanding of the Fe biogeochemical cycle in the Southern Ocean and provide a key reference for future observational and modelling efforts.

CRediT authorship contribution statement

V. Coussy: Writing – original draft, Investigation, Data curation, Conceptualization. **J.M. Santana-Casiano:** Writing – review & editing, Funding acquisition, Conceptualization. **M. González-Dávila:** Writing – review & editing. **D. González-Santana:** Writing – review & editing. **T. N. Mtshali:** Writing – review & editing, Investigation. **T.J. Ryan-Keogh:** Writing – review & editing, Investigation. **S. Samanta:** Investigation. **A.N. Roychoudhury:** Investigation. **A.G. González:** Writing – review & editing, Supervision, Funding acquisition, Data curation, Conceptualization.

Declaration of competing interest

The authors declare that they have no known competing financial interests or personal relationships that could have appeared to influence the work reported in this paper.

Acknowledgments

We would like to acknowledge the support and assistance of the captain and crew of the R/V SA Agulhas II, along with all the trace metal sampling teams. The research expedition and the research conducted on the vessel were part of a South African initiative to complete a seasonal cycle study (Southern oCean seAsonal cycLe Experiment (SCALE)), funded by the National Research Foundation (NRF) of South Africa under the South African National Antarctic Programme (SANAP). TJRK and TNM were supported through the CSIR's Southern Ocean Carbon and Climate Observatory (SOCCO) Programme (http://socco.org.za/), funded by the Department of Science, Technology and Innovation (DST/CON 0182/2017) and the CSIR's Parliamentary Grant. We would like to acknowledge funding received from the NRF SANAP, South Africa, grant number 129230. The trace metal sampling and analytical work was supported by a grant to AR from a charitable donor as part of the Whales and Climate Change Program (whalesandclimate.org). Part of this study was funded by the FeRIA (PID2021-123997NB-I00) project from the Ministerio de Ciencia e Innovación (Spain). Additional support was provided by the PROTEA programme (FSTR1804183 22331, SeaTraM-PROTEA project, PI: E. Bucciarelli) for the winter cruise and by LEMAR for the spring cruise.

Appendix A. Supplementary data

Supplementary data to this article can be found online at https://doi.org/10.1016/j.marenvres.2026.107987.

Data availability

Data will be made available on request.

References

Ardiningsih, I., Seyitmuhammedov, K., Sander, S.G., Stirling, C.H., Reichart, G.J., Arrigo, K.R., Gerringa, L.J.A., Middag, R., 2021. Fe-binding organic ligands in coastal and frontal regions of the western Antarctic Peninsula. Biogeosciences 18, 4587–4601. https://doi.org/10.5194/BG-18-4587-2021.

Arnone, V., González-Santana, D., González-Dávila, M., González, A.G., Santana-Casiano, J.M., 2022. Iron and copper complexation in Macaronesian coastal waters. Mar. Chem. 240, 104087. https://doi.org/10.1016/J.MARCHEM.2022.104087.

Arnone, V., Santana-Casiano, J.M., González-Dávila, M., Planquette, H., Sarthou, G., Gerringa, L.J.A., González, A.G., 2023. Natural copper-binding ligands in the Arctic Ocean. The influence of the transpolar drift (GEOTRACES GN04). Front. Mar. Sci. 10, 1306278. https://doi.org/10.3389/FMARS.2023.1306278/PDF.

Boyd, P.W., Jickells, T., Law, C.S., Blain, S., Boyle, E.A., Buesseler, K.O., Coale, K.H., Cullen, J.J., de Baar, H.J.W., Follows, M., Harvey, M., Lancelot, C., Levasseur, M., Owens, N.P.J., Pollard, R., Rivkin, R.B., Sarmiento, J., Schoemann, V., Smetacek, V., Takeda, S., Tsuda, A., Turner, S., Watson, A.J., 1979. Mesoscale iron enrichment experiments 1993-2005: synthesis and future directions. Science 315, 612–617. https://doi.org/10.1126/science.1131669, 2007.

Boye, M., van den Berg, C.M.G., de Jong, J.T.M., Leach, H., Croot, P., de Baar, H.J.W., 2001. Organic complexation of iron in the Southern Ocean. Deep-Sea Res. Part I Oceanogr. Res. Pap. 48, 1477–1497. https://doi.org/10.1016/S0967-0637(00)00099-6.

Boye, M., Nishioka, J., Croot, P.L., Laan, P., Timmermans, K.R., de Baar, H.J.W., 2005. Major deviations of iron complexation during 22 days of a mesoscale iron enrichment in the open Southern Ocean. Mar. Chem. 96, 257–271. https://doi.org/10.1016/j.marchem.2005.02.002.

Croot, P.L., Johansson, M., 2000. Determination of iron speciation by cathodic stripping voltammetry in seawater using the competing ligand 2-(2-Thiazolylazo)-p-cresol (TAC). Electroanalysis 12, 565–576. https://doi.org/10.1002/(SICI)1521-4109(200005)12:8<565::AID-ELAN565>3.0.CO;2-L.

Croot, P.L., Andersson, K., Öztürk, M., Turner, D.R., 2004. The distribution and speciation of iron along 6°E in the Southern Ocean. Deep Sea Res. Part II Top. Stud. Oceanogr. 51, 2857–2879. https://doi.org/10.1016/j.dsr2.2003.10.012.

Cutter, G.A., Bruland, K.W., 2012. Rapid and noncontaminating sampling system for trace elements in global ocean surveys. Limnol Oceanogr. Methods 10, 425–436. https://doi.org/10.4319/LOM.2012.10.425.

Cutter, G., Casciotti, K., Croot, P., Geibert, W., Geochemistry, M., Heimbürger, L.-E., Lohan, M., Planquette, H., van de Flierdt, T., 2017. Sampling and sample-handling protocols for GEOTRACES cruises. https://doi.org/10.25607/OBP-2.

Demasy, C., Boye, M., Lai, B., Burckel, P., Feng, Y., Losno, R., Borensztajn, S., Besson, P., 2024. Iron dissolution from Patagonian dust in the Southern Ocean: under present and future conditions. Front. Mar. Sci. 11, 1363088. https://doi.org/10.3389/FMARS.2024.1363088/PDF.

Duan, Y., Ao, J., Waerenborgh, C., Clemente-Juan, J.M., Giménez, C., Giménez-Saiz, G., Coronado, E., 2017. Light-induced decarboxylation in a photo-responsive iron-containing complex based on polyoxometalate and oxalato ligands. Chem. Sci. https://doi.org/10.1039/c6sc01919f.

Geider, R.J., 1999. Complex lessons of iron uptake. Nature 400, 815–816. https://doi.org/10.1038/23582.

Genovese, C., Grotti, M., Ardini, F., Corkill, M., Duprat, L., Wuttig, K., Townsend, A., Lannuzel, D., 2022. A proposed seasonal cycle of dissolved iron-binding ligands in Antarctic sea ice. Elem Sci Anth. https://doi.org/10.1525/ELEMENTA.2021.00030.

Gerringa, L.J.A., Veldhuis, M.J.W., Timmermans, K.R., Sarthou, G., de Baar, H.J.W., 2006. Co-variance of dissolved Fe-binding ligands with phytoplankton characteristics in the Canary Basin. Mar. Chem. 102, 276–290. https://doi.org/10.1016/j.marchem.2006.05.004.

Gerringa, L.J.A., Blain, S., Laan, P., Sarthou, G., Veldhuis, M.J.W., Brussaard, C.P.D., Viollier, E., Timmermans, K.R., 2008. Fe-binding dissolved organic ligands near the Kerguelen Archipelago in the Southern Ocean (Indian sector). Deep Sea Res. Part II Top. Stud. Oceanogr. 55, 606–621. https://doi.org/10.1016/j.dsr2.2007.12.007.

Gerringa, L.J.A., Gledhill, M., Ardiningsih, I., Muntjewerf, N., Laglera, L.M., 2021. Comparing CLE-AdCSV applications using SA and TAC to determine the Fe-binding characteristics of model ligands in seawater. Biogeosciences 18, 5265–5289. https://doi.org/10.5194/bg-18-5265-2021.

Gledhill, M., Buck, K.N., 2012. The organic complexation of iron in the marine environment: a review. Front. Microbiol. 3, 18807. https://doi.org/10.3389/FMICB.2012.00069/BIBTEX.

Gledhill, M., Gerringa, L.J.A., 2017. The effect of metal concentration on the parameters derived from complexometric titrations of trace elements in seawater—A model study. Front. Mar. Sci. 4. https://www.frontiersin.org/articles/10.3389/fmars.2017.00254.

Hassler, C.S., Schoemann, V., Nichols, C.M., V Butler, E.C., Boyd, P.W., 2011. Saccharides enhance iron bioavailability to Southern Ocean phytoplankton. Proc. Natl. Acad. Sci. U.S.A 108, 1076–1081. https://doi.org/10.1073/pnas.1010963108.

Hassler, C.S., Simó, R., Fawcett, S.E., Ellwood, M.J., Jaccard, S.L., 2025. Marine biogenic humic substances control iron biogeochemistry across the Southern Ocean. Nat. Commun. 16, 1–11. https://doi.org/10.1038/S41467-025-57491-5. SUBJMETA.

Klunder, M.B., Laan, P., Middag, R., De Baar, H.J.W., van Ooijen, J.C., 2011. Dissolved iron in the Southern Ocean (Atlantic sector). Deep Sea Res. Part II Top. Stud. Oceanogr. 58, 2678–2694. https://doi.org/10.1016/j.dsr2.2010.10.042.

Klunder, M.B., Laan, P., De Baar, H.J.W., Middag, R., Neven, I., Van Ooijen, J., 2014. Dissolved Fe across the Weddell Sea and Drake Passage: impact of DFe on nutrient uptake. Biogeosciences 11, 651–669. https://doi.org/10.5194/BG-11-651-2014.

Lacan, F., Radic, A., Jeandel, C., Poitrasson, F., Sarthou, G., Pradoux, C., Freydier, R., 2008. Measurement of the isotopic composition of dissolved iron in the open ocean. Geophys. Res. Lett. 35. https://doi.org/10.1029/2008GL035841.

Lucia, M., Campos, A.M., van den Berg, C.M.G., 1994. Determination of copper complexation in sea water by cathodic stripping voltammetry and ligand competition with salicylaldoxime. Anal. Chim. Acta 284, 481–496. https://doi.org/10.1016/0003-2670(94)85055-0.

Marsay, C.M., Sedwick, P.N., Dinniman, M.S., Barrett, P.M., Mack, S.L., D Jr., J.M., 2014. Estimating the benthic efflux of dissolved iron on the Ross Sea continental shelf. Geophys. Res. 41, 7576–7583. https://doi.org/10.1002/2014GL061684.

Moore, J.K., Doney, S.C., Glover, D.M., Fung, I.Y., 2001. Iron cycling and nutrient-limitation patterns in surface waters of the world ocean. Deep Sea Res. Part II Top. Stud. Oceanogr. 49, 463–507. https://doi.org/10.1016/S0967-0645(01)00109-6.

Nicholson, S.A., Lévy, M., Jouanno, J., Capet, X., Swart, S., Monteiro, P.M.S., 2019. Iron supply pathways between the surface and subsurface waters of the Southern Ocean: from winter entrainment to summer storms. Geophys. Res. Lett. 46, 14567–14575. https://doi.org/10.1029/2019GL084657.

Omanović, D., Garnier, C., Pižeta, I., 2015. ProMCC: an all-in-one tool for trace metal complexation studies. Mar. Chem. 173, 25–39. https://doi.org/10.1016/j.marchem.2014.10.011.

Orsi, A.H., Whitworth, T., Nowlin, W.D., 1995. On the meridional extent and fronts of the antarctic circumpolar current. Deep-Sea Res. Part I Oceanogr. Res. Pap. 42, 641–673. https://doi.org/10.1016/0967-0637(95)00021-W.

Pollard, R.T., Salter, I., Sanders, R.J., Lucas, M.I., Moore, C.M., Mills, R.A., Statham, P.J., Allen, J.T., Baker, A.R., Bakker, D.C.E., Charette, M.A., Fielding, S., Fones, G.R., French, M., Hickman, A.E., Holland, R.J., Hughes, J.A., Jickells, T.D., Lampitt, R.S., Morris, P.J., Nédélec, F.H., Nielsdóttir, M., Planquette, H., Popova, E.E., Poulton, A. J., Read, J.F., Seeyave, S., Smith, T., Stinchcombe, M., Taylor, S., Thomalla, S., Venables, H.J., Williamson, R., V Zubkov, M., 2009. Southern Ocean deep-water carbon export enhanced by natural iron fertilization. Nature 457, 577–580. https://doi.org/10.1038/nature07716.

Poorvin, L., Sander, S.G., Velasquez, I., Ibisanmi, E., LeCleir, G.R., Wilhelm, S.W., 2011. A comparison of Fe bioavailability and binding of a catecholate siderophore with virus-mediated lysates from the marine bacterium Vibrio alginolyticus PWH3a. J. Exp. Mar. Biol. Ecol. 399, 43–47. https://doi.org/10.1016/j.jembe.2011.01.016.

Ramalepe, T., Samanta, S., Cloete, R., Ryan-Keogh, T.J., Roychoudhury, A.N., 2024. Winter entrainment drives the mixed layer supply of manganese in the Southern Ocean. Limnol. Oceanogr. 69, 1929–1940. https://doi.org/10.1002/LNO.12634.

Rico, M., López, A., Santana-Casiano, J.M., Gonzàlez, A.G., Gonzàlez-Dàvila, M., 2013. Variability of the phenolic profile in the diatom Phaeodactylum tricornutum growing under copper and iron stress. Limnol. Oceanogr. 58, 144–152. https://doi.org/10.4319/lo.2013.58.1.0144.

Ringard, A., Planquette, H., Mtshali, T., Roychoudhury, A., Bucciarelli, E., 2025. Particulate iron seasonality between winter and spring in the open Southern Atlantic Ocean is primarily driven by non-biological processes. Mar. Chem. 272, 104552. https://doi.org/10.1016/J.MARCHEM.2025.104552.

Rintoul, S.R., Hughes, C.W., Olbers, D., 2001. Chapter 4.6 the antarctic circumpolar current system. In: Int. Geophys. Academic Press, pp. 271–302. https://doi.org/10.1016/S0074-6142(01)80124-8.

Rio, M.H., Guinehut, S., Larnicol, G., 2011. New CNES-CLS09 global mean dynamic topography computed from the combination of GRACE data, altimetry, and in situ measurements. J. Geophys. Res., Oceans 116, 7018. https://doi.org/10.1029/2010JC006505.

Rue, E.L., Bruland, K.W., 1995. Complexation of iron(III) by natural organic ligands in the central North Pacific as determined by a new competitive ligand equilibration/adsorptive cathodic stripping voltammetric method. Mar. Chem. 50, 117–138. https://doi.org/10.1016/0304-4203(95)00031-L.

Ryan-Keogh, T., 2025a. SCALE-SPR19 trace metal clean CTD rosette data. https://doi.org/10.5281/ZENODO.15195846usingtheDOI10.5281/zenodo.5906680.

Ryan-Keogh, T., 2025b. SCALE-WIN19 trace metal clean rosette data. https://doi.org/10.5281/ZENODO.15195978.

Samanta, S., Cloete, R., Loock, J., Rossouw, R., Roychoudhury, A.N., 2021. Determination of trace metal (Mn, fe, ni, cu, zn, co, cd and pb) concentrations in seawater using single quadrupole icp-ms: a comparison between offline and online preconcentration setups. Minerals 11, 1289. https://doi.org/10.3390/MIN11111289/S1.

Santana-Casiano, J.M., González-Dávila, M., González, A.G., Rico, M., López, A., Martel, A., 2014. Characterization of phenolic exudates from *Phaeodactylum tricornutum* and their effects on the chemistry of Fe(II)–Fe(III). Mar. Chem. 158, 10–16. https://doi.org/10.1016/j.marchem.2013.11.001.

Sarmiento, J.L., Gruber, N., Brzezinski, M.A., Dunne, J.P., 2004. High-latitude controls of thermocline nutrients and low latitude biological productivity. Nature 427, 56–60. https://doi.org/10.1038/nature02127.

Sato, M., Takeda, S., Furuya, K., 2007. Iron regeneration and organic iron(III)-binding ligand production during in situ zooplankton grazing experiment. Mar. Chem. 106, 471–488. https://doi.org/10.1016/j.marchem.2007.05.001.

Smith, A.J.R., Nelson, T., Ratnarajah, L., Genovese, C., Westwood, K., Holmes, T.M., Corkill, M., Townsend, A.T., Bell, E., Wuttig, K., 2022. Identifying potential sources of iron-binding ligands in coastal Antarctic environments and the wider Southern Ocean. Front. Mar. Sci. 9, 948772. https://doi.org/10.3389/fmars.2022.948772.

Swart, S., Speich, S., Ansorge, I.J., Lutjeharms, J.R.E., 2010. An altimetry-based gravest empirical mode south of Africa: 1. Development and validation. J. Geophys. Res., Oceans 115, 3002. https://doi.org/10.1029/2009JC005299.

Tagliabue, A., Sallée, J.-B., Bowie, A.R., Lévy, M., Swart, S., Boyd, P.W., 2014. Surface-water iron supplies in the Southern Ocean sustained by deep winter mixing. Nat. Geosci. 7, 314–320. https://doi.org/10.1038/ngeo2101.

Tagliabue, A., Bowie, A.R., DeVries, T., Ellwood, M.J., Landing, W.M., Milne, A., Ohnemus, D.C., Twining, B.S., Boyd, P.W., 2019. The interplay between regeneration and scavenging fluxes drives ocean iron cycling. Nat. Commun. 10, 4960. https://doi.org/10.1038/s41467-019-12775-5.

Thomalla, S.J., Nicholson, S.A., Ryan-Keogh, T.J., Smith, M.E., 2023. Widespread changes in Southern Ocean phytoplankton blooms linked to climate drivers. Nat. Clim. Change 13, 975–984. https://doi.org/10.1038/s41558-023-01768-4.

Thuróczy, C.-E., Gerringa, L.J.A., Klunder, M.B., Laan, P., de Baar, H.J.W., 2011. Observation of consistent trends in the organic complexation of dissolved iron in the Atlantic sector of the Southern Ocean. Deep Sea Res. Part II Top. Stud. Oceanogr. 58, 2695–2706. https://doi.org/10.1016/j.dsr2.2011.01.002.

Witter, A.E., Hutchins, D.A., Butler, A., Luther, G.W., 2000. Determination of conditional stability constants and kinetic constants for strong model Fe-binding ligands in seawater. Mar. Chem. 69, 1–17. https://doi.org/10.1016/S0304-4203(99)00087-0.